Mineralogy and Petrology (2020) 114:289–303
https://doi.org/10.1007/s00710-020-00707-x

ORIGINAL PAPER

Zircon U-Pb ages, geochemistry and isotopic characteristics of the Chu Lai granitic pluton in the Kontum massif, central Vietnam

Nguyen Trung Minh[1,2] · Nguyen Thi Dung[1] · Doan Dinh Hung[1,2] · Pham Minh[3,4] · Yongjae Yu[5] · Pham Trung Hieu[3,4]

Received: 2 May 2018 / Accepted: 6 April 2020 / Published online: 8 May 2020

Abstract

The Chu Lai granite is widespread throughout the northern Kontum massif and is an important key in understanding the evolution of the Kontum region and its vicinity. The study presents new data on geochemistry, zircon U-Pb ages, and Nd-Hf isotopes from the Chu Lai granite which allows to constrain the Paleozoic tectonic evolution of the Kontum massif. The Chu Lai granite contains alumina-rich minerals (garnet and muscovite), is depleted in Ba, Nb, Ta, Sr and Ti but enriched in Rb, Th, U and Pb. These geochemical characteristics indicate a S-type nature of the Chu Lai granite. The zircon ε_{Hf} values vary between −16.7 to −1 and Hf model ages (T_{DM2}) between 1.50 and 2.49 Ga as well as whole rock ε_{Nd} values of −8.3 to −5.8 and Nd model ages (T_{DM2}) between 1.67 and 1.89 Ga. The Hf-Nd isotope data indicate that the Chu Lai granite was derived from partial melting of Paleoproterozoic metasedimentary material. The LA-ICP-MS zircon U-Pb ages range from 445 Ma to 454 Ma, suggesting a crystallization of the Chu Lai granite during the Ordovician-Silurian period.

Keywords Zircon U-Pb age · Hf isotope · Geochemistry · S-type granite · central Vietnam

Introduction

The tectonic evolution of Southeast Asia has been controlled by sequential accreting of a number of continental blocks such as South China, Indochina, and Sibumasu (Metcalfe 2013).

Editorial handling: C. Hauzenberger

Electronic supplementary material The online version of this article (https://doi.org/10.1007/s00710-020-00707-x) contains supplementary material, which is available to authorized users.

✉ Pham Trung Hieu
pthieu@hcmus.edu.vn

[1] Viet Nam National Museum of Nature, Vietnam Academy of Science and Technology (VAST), 18 Hoang Quoc Viet, Cau Giay, Ha Noi, Vietnam

[2] Graduate University of Science and Technology, VAST, 18 Hoang Quoc Viet, Cau Giay, Ha Noi, Vietnam

[3] Faculty of Geology, VNU-HCM University of Science, 227 Nguyen Van Cu Street, Ho Chi Minh, Vietnam

[4] Vietnam National University Ho Chi Minh city, Ho Chi Minh, Vietnam

[5] Department of Geology and Earth Environmental Sciences, Chungnam National University, Daejeon 305-764, Republic of Korea

The South China block comprises the Cathaysia and Yangtze blocks, which were welded together along the Jiangnan Orogen (Yu et al. 2008; Zhang et al. 2012). In particular, the Indochina block, derived from northern Gondwanaland, is the largest continental craton of Southeast Asia (Metcalfe 2013; Hieu et al. 2009, 2017). It is recognized that the Truong Son belt and Kontum massif are part of the Indosinian mountain system (Fig. 1; Roger et al. 2007; Hieu et al. 2017). According to Hutchison (1989), the formation of the Kontum massif is considered as an Archean core complex of the Indochina block. On the other hand, the Kontum massif can be explained as reworked crust formed by post-collisional magmatism or metamorphism (Owada et al. 2007).

Two collisional events were identified in the Kontum massif. An earlier collisional event occurred in the Ordovician-Silurian (Table 1) (Nagy et al. 2001; Roger et al. 2007; Nakano et al. 2013; Tran et al. 2014; Hieu et al. 2016). A later collisional event occurred in the Permian-Triassic (Lan et al. 2000; Nakano et al. 2007, 2013; Hieu et al. 2015). The former Ordovician-Silurian event is assumed to be linked to arc magmatism (Nagy et al. 2001), an early extension breakup of Gondwana (Carter et al. 2001) as well as the result of intracontinental orogenic processes (Nagy et al. 2001; Usuki et al. 2009). The later collisional event during Permian-Triassic times resulted in subduction-induced

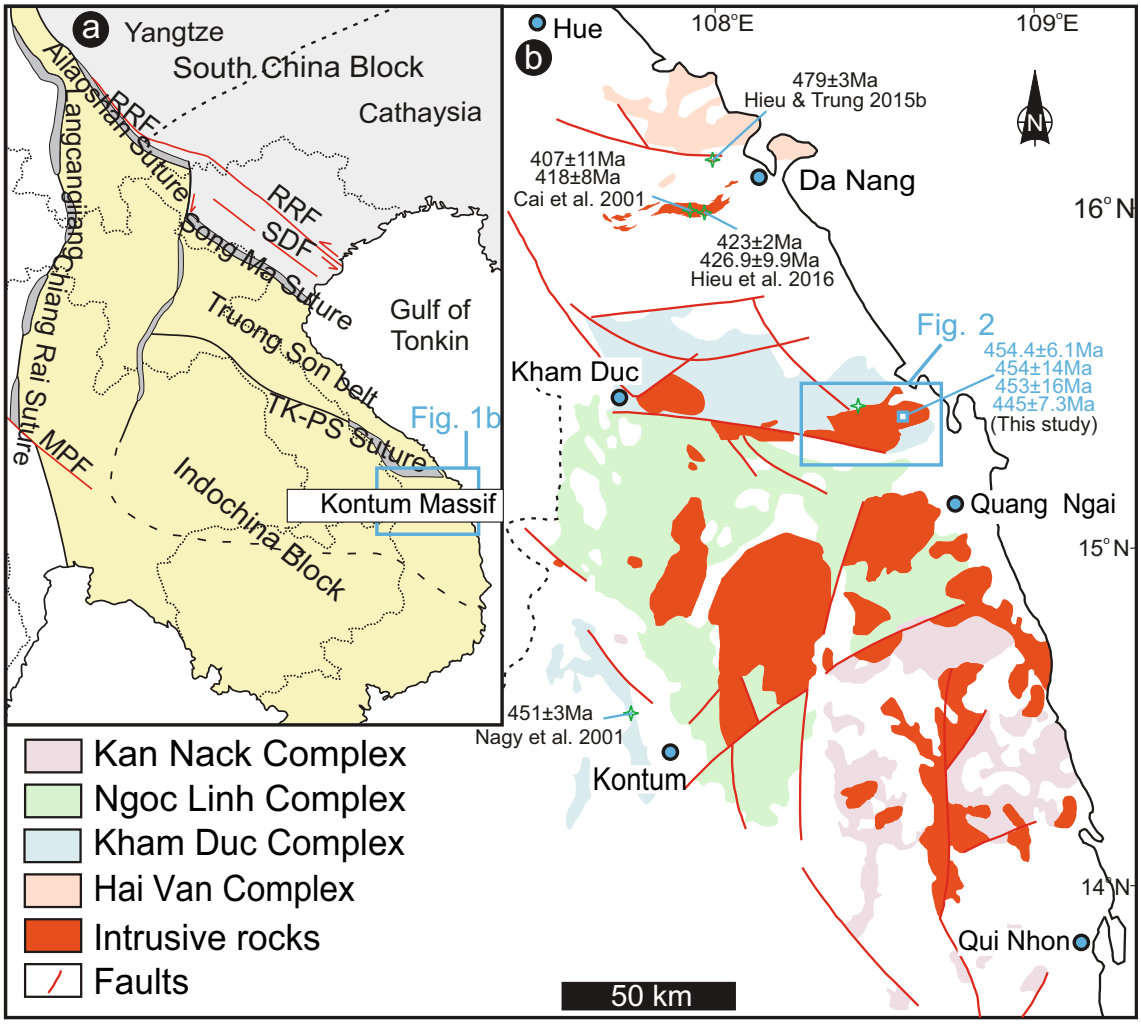

Fig. 1 Geological sketch map of the Indochina block. a Index map (modified after Thuc and Trung 1995; Shi et al. 2015). b study area (modified after Hieu et al. 2016)

metamorphism and exhumation at the East Asian Continental Margin.

Recent studies have suggested that tectonic activity in the Kontum massif is also associated with subduction and collision during the Ordovician-Silurian (Tran et al. 2014; Shi et al. 2015; Hieu et al. 2016). In this article, we present early Paleozoic records from the Chu Lai granite of the Kontum massif in central Vietnam.

Table 1 Ages of Ordovician-Silurian granitic rocks in Kontum massif. Locations are displayed in Fig. 1b

Sample. no	Rock type	Location	Age (Ma)	Method	Material	Reference
V1722	Granitic gneiss	Chu Lai	445 ± 7.3	LA-ICP-MS	zircon	This study
V1723	Granitic gneiss	Chu Lai	453 ± 16	LA-ICP-MS	zircon	This study
V1724	Granitic gneiss	Chu Lai	454.4 ± 6.1	LA-ICP-MS	zircon	This study
V1726	Granitic gneiss	Chu Lai	454 ± 14	LA-ICP-MS	zircon	This study
DLT02	Granite	Dai Loc	426.9 ± 9.9	LA-ICP-MS	zircon	Hieu et al. (2016)
DLT07	Granite	Dai Loc	423 ± 2	LA-ICP-MS	zircon	Hieu et al. (2016)
V1104	Quartz diorite	Ben Giang	479 ± 3	LA-ICP-MS	zircon	Hieu et al. (2015)
VN13	Gneiss	Dai Loc	407 ± 11	SHRIMP	zircon	Carter et al. (2001)
VN610	Gneiss	Dai Loc	418 ± 8	SHRIMP	zircon	Carter et al. (2001)
VN386	Granodiorite	Poko River	451 ± 3	LA-ICP-MS	zircon	Nagy et al. (2001)

Geological background

The Kontum massif is located in the southern the Truong Son belt and the boundary of them is the Tam Ky – Phuoc Son suture (Fig. 1a). The Tam Ky-Phuoc Son suture is a major collisional structure in central Vietnam, and have experienced multiple deformational events. The Tam Ky – Phuoc Son suture contains strongly dismembered, sheared and serpentinized ultramafic bodies (Tran et al. 2014) which are scattered hundreds of kilometer along strike. Recently, some Vietnamese and foreign geologists consider that the bodies in the Tam Ky-Phuoc Son suture are considered to be remnants of ancient oceanic crust (Tran et al. 2014; Shi et al. 2015). The Tam Ky-Phuoc Son suture formed via the closure of an ancient Paleotethyan ocean basin through terrane assembly during the Ordovician–Silurian time along the Gondwana margin. Granitoids in the Truong Son belt can be divided mainly into two events based on petrological studies, geochemistry zircon U–Pb ages and Nd–Hf isotopic compositions: the first event is characterized by Ordovician-Silurian rocks (Dien Binh, Ben Giang – Que. Son, and Dai Loc granitoids) and the second event displays late Permian-early Triassic rocks (the Hai Van, and Deo Ca granitoids) (Nakano et al. 2013; Hieu et al. 2016). The Dai Loc granitoid shows features of I–type granite and displays subduction–related geochemical features in the Ordovician-Silurian time (Hieu et al. 2016). The Permian-Triassic igneous rocks were considered to be created in subduction prior to the South China and Indochina collision (Thanh et al. 2019).

The Kontum massif is considered as the basement of the Indochina block (Fig. 1a). It is dominated by metamorphic rocks of varying metamorphic grade ranging from low-grade schist to high-grade granulite (Osanai et al. 2004; Nakano et al. 2007, 2013; Hieu et al. 2016). Examples of these metamorphic basement rocks can be found in the Kan Nack Complex, Ngoc Linh Complex, and Kham Duc Complex (Tri and Khuc 2011) (Fig. 1b). In the southeastern part of the Kontum massif, the Kan Nack Complex includes mafic charnockitic-enderbitic gneiss, granulite facies metapelite which is composed of the mineral assemblage garnet-cordierite-hypersthene as well as some calc-silicate rock. The Kan Nack rocks were formed by ultra-high temperature (UHT) metamorphism at 900-990 °C and 1.03–1.50 GPa (Nakano et al. 2007). The evidence of this high-grade metamorphism is the occurrences of garnet–cordierite–sillimanite–biotite gneiss in the eastern Kan Nack Complex. In the light of monazite age dating, the main metamorphic events took place at ~426 Ma and a younger metamorphic event at ~239 Ma (Nakano et al. 2013).

In the northwestern part of the Kontum massif, the Ngoc Linh Complex consists of mainly lower granulite facies rocks, mainly schist, amphibole gneiss, biotite gneiss, amphibolite, and granulite. Its garnet-biotitic gneiss underwent metamorphism at 700 °C at 0.5 GPa (Nakano et al. 2007).

In the southwestern and northern parts of the Kontum massif, the Kham Duc Complex is composed of amphibolite, amphibole gneiss, and biotite gneiss. The Kham Duc complex unconformably underlays the Ngoc Linh complex and the Cambrian-Silurian sedimentary rocks. Based on the occurrence of muscovite, kyanite, and staurolite (Nakano et al. 2007), the Kham Duc complex consists of low to medium pressure (0.79–0.89 GPa) and medium to high temperature (570-700 °C) metamorphic rocks. The metamorphic rocks in the Silurian-Ordovician event are not only found in the Kan Nack complex and the Ngoc Linh Complex but also in the Kham Duc Complex. Based on field evidence, the Chu Lai Complex intrudes into the Kham Duc metamorphic rocks and caused the main migmatization.

The Kan Nack Complex was initially proposed to belong to an Archean terrane based on global lithologic similarity (Tri and Khuc 2011). Previous studies of metamorphic rocks showed metamorphic ages at 243–260 Ma from U-Pb zircon age dating (Carter et al. 2001; Nagy et al. 2001; Nam et al. 2004). However, recent geochronologic results indicate that the Kontum massif experienced a two-stage evolution: the former occurred in the Ordovician-Silurian (Nagy et al. 2001; Roger et al. 2007; Nakano et al. 2013; Tran et al. 2014; Hieu et al. 2016) and the latter happened in the Permian-Triassic (e.g. Hai Van Complex) (Hoa et al. 2008; Nakano et al. 2007, 2013; Hieu et al. 2015).

The Chu Lai Complex covers an E-W trending area of about 480 km^2 (Fig. 2 and 3a) in the northern and western parts of the Kontum massif and in the southern of the Truong Son belt. The Chu Lai intrusion's is main exposure is found in the south of Tam Ky town (Fig. 2). The Chu Lai intrusion is surrounded by metamorphic rocks of amphibolite-facies that belong to the Kham Duc formation (Tri and Khuc 2011). The Chu Lai granite cuts the Kham Duc formation along its western side. The boundary between the Chu Lai granite and the Kham Duc formation is often unclear, which is a transitional zone composed of meta-sedimentary rocks to migmatite and granitic gneiss. This indicates a gradual transition between igneous and metamorphic rocks. Cambrian-Silurian sedimentary rocks unconformably cover the Chu Lai granite (Fig. 2). In the Chu Lai intrusion, there are abundant xenoliths of meta-sedimentary rocks from Kham Duc complex and with micro-folded structures. In one outcrop, the Chu Lai granite commonly contains xenoliths of meta-sedimentary rocks (Fig. 3b).

Sample preparation and analytical methods

Bulk rock samples weighing at least 5 kg each were collected by the authors during fieldwork Summer 2017. Weathered and discolored sample parts were removed in the laboratory using a water-cooled diamond blade. Standard sized 27 × 47 mm thin and polished sections were prepared using silicon carbide

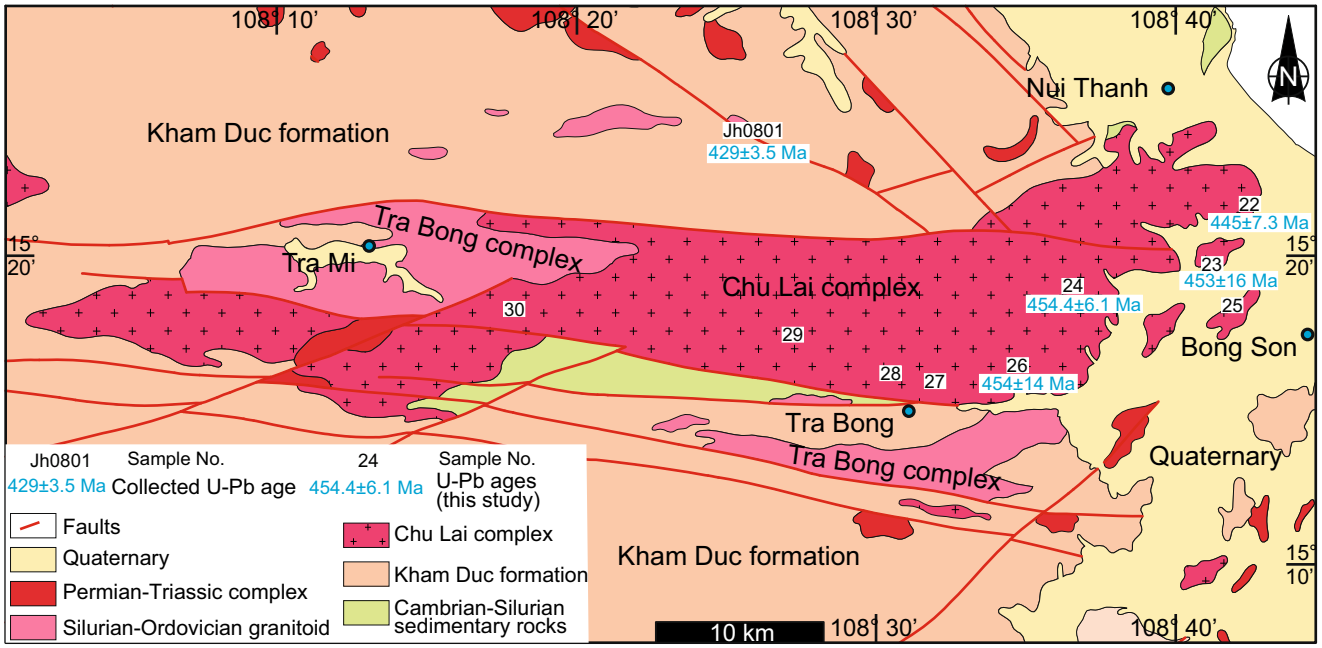

Fig. 2 Simplified geological map of the Kontum massif (modified after DGMVN, 1995). Ages according to Tran et al. (2014). Sample numbers refer to Tables 2 and 3

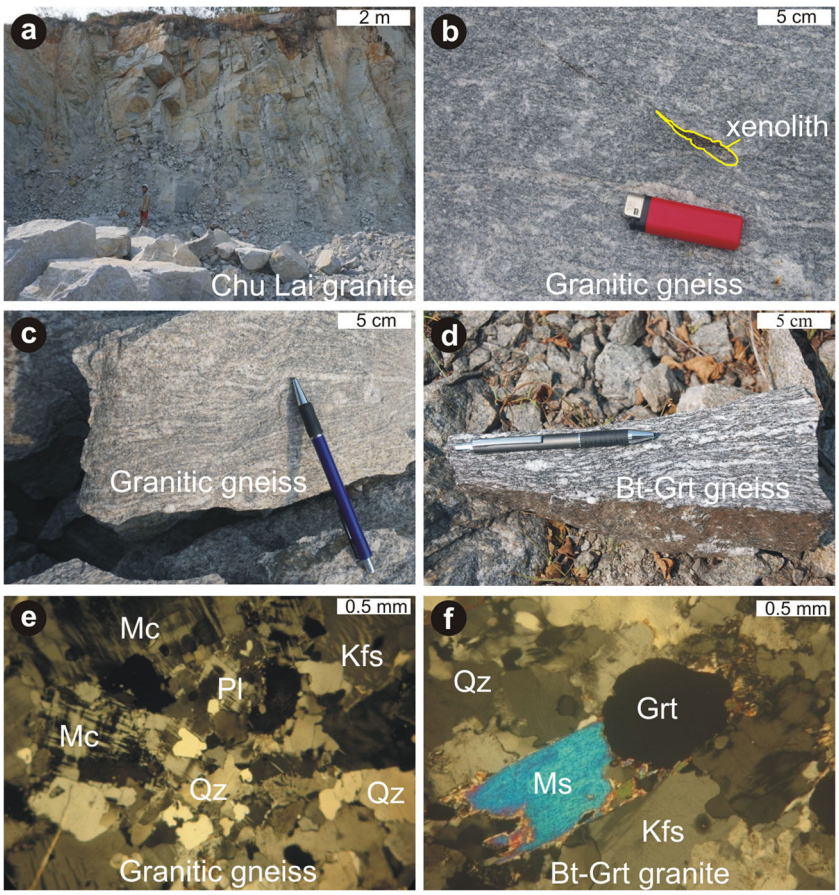

Fig. 3 Field photos and thin-section photomicrographs from the Chu Lai pluton: a massive granite, b Outcrop of the Chu Lai Bt-Grt granite, c and d thin section images. Mineral names abbreviated cf. Whitney and Evans (2010)

slurries following routine procedures modified after Humphries (1992). Thin sections for optical petrography were finished at 30 μm thickness and covered with a 0.17 mm glass cover slip, and were assessed in a Zeiss Axioskop 40A-pol in transmitted polarized light. Mineral modal contents were determined in vol% by point counting minimum twelve-hundred points per thin section, using a Prior Scientific device mounted to the rotating stage.

Bulk sample materials without visible weathering were comminuted in a jaw breaker to pass 0.5 mm. Heavy minerals concentrates were prepared by initial magnetic and heavy-liquid separation techniques, zircon grains were handpicked from these concentrates under a stereomicroscope. Selected grains were mounted on double-sided adhesive tape, embedded in Struers Epofix epoxy to form a Ø25mm block, and polished with diamond pastes 6–3–1-0.25 μm to expose the interior and center of the grains.

Internal growth zoning in polished zircon grains was assessed by cathodo-luminescence (CL) analysis in a Zeiss LEO VP1450 scanning electron microscope (SEM), operated at 15 kV and 500pA beam current in low vacuum (25 Pa) to minimize charging. Selected CL images are collated in Fig. 7.

Zircon U-Pb dating was carried out with a laser ablation – inductively coupled plasma – mass spectrometer (LA-ICP-MS) at the State Key Laboratory of Geological Processes and Mineral Resources, China University of Geosciences, Wuhan. Detailed operating conditions of the LA-ICP-MS as well as data reduction protocols are described in Liu et al. (2008, 2010), but have been modified regarding standard settings in order to analyse U-Pb dating. A GeoLas 2005 laser-ablation system an Agilent 7500a ICP-MS was performed with a laser repetition of 6 Hz and a laser spot size of 32 μm. Helium gas was used to transport the ablated sample to the ICP-MS torch from the ablation cell. Quantitative calibration of U-Pb dating was performed with the ICPMSDataCal software (Liu et al. 2008, 2010). The measured ratio of $^{206}Pb/^{238}U$ was calibrated based on the standard zircon 91,500 (Wiedenbeck et al. 1995).

Four samples from Chu Lai granite were selected for Sm-Nd isotopic analyses. Analyses of whole-rock Sm-Nd isotopes were done at the University of Science and Technology of China in Hefei. Detailed analyses were described in Chen et al. (2000, 2007).

Zircon Hf isotope analyses were performed with a Nu Plasma multi-collector ICP-MS equipped with a Geolas-2005 193 nm ArF excimer laser at the IGG CAS. These analyses were performed with a spot size of 44 μm and a laser repetition rate of 10 Hz. Descriptions on the analytical procedures and the interference correction method of $^{176}Yb/^{176}Hf$ are described in Wu et al. (2006), with slight modifications regarding regarding standard settings in order to analyse zircon Hf isotope composition. We assumed a decay constant of 1.865×10^{-11} a^{-1} for ^{176}Lu (Scherer et al. 2001). Chondritic values of $^{176}Lu/^{177}Hf = 0.0336$ and $^{176}Hf/^{177}Hf = 0.282785$ were used for the calculation of ε_{Hf} (Iizuka et al. 2017). The single stage model age (T_{DM1}) was calculated with the depleted mantle reservoir with present-day value of $^{176}Hf/^{177}Hf = 0.28325$ and $^{176}Lu/^{177}Hf = 0.0384$ (Iizuka et al. 2017). The two-stage Hf model age (T_{DM2}) was calculated based on $^{176}Lu/^{177}Hf = 0.015$ for the average continental crust (Iizuka et al. 2017). The analytical results are shown in Table S3.

Nine samples from Chu Lai granite were selected for whole-rock geochemical analyses. Main and trace elements were analyzed by X-ray fluorescence (XRF) and inductively coupled plasma – mass spectrometry (ICP-MS) at the Institute of Geology and Geophysics, Chinese Academy of Sciences (IGG CAS).Comminuted non-weathered bulk sample material (see above) was pulverized in an agate-lined mill to pass 200 mesh (<75 μm). For main element analysis by X-ray fluorescence (XRF), 0.5 ± 0.0005 g sample powder was blended with 10× excess Li-borate flux and digested at ~1050 °C in a 95Pt5Au crucible to form a glass bead for analysis. The Rh-tube in the PANalytical Axios Mineral XRF instrument was operated at 40 kV and 40 mA. Raw element content data were ZAF corrected using proprietary PANalytical software and recalculated to oxides assuming stoichiometry; total iron content is represented as Fe_2O_3. Loss on ignition (LOI) was determined gravimetrically on separate powder aliquots pre-dried at 105 °C to remove absorbed molecular water. Lower limits of detection (LLD) are listed per main element oxide species in a separate column in Table 2. Analytical sum totals for main element oxides are within 100.00 ± 1.50 wt% indicating good quality results.

For trace element analysis by ICP-MS, a separate aliquot of 0.5 ± 0.0005 g sample powder is weighed into a PTFE-lined steel vessel for digestion in 20 mL of $1HNO_3$:4HF excess concentrated acid. The closed vessel is heated at 195 °C for 48 h and allowed to cool to room temperature. Subsequently, the open vessel is evaporated at 145 °C to incipient dryness then cooled to room temperature, added 2 mL of distilled 1 N HNO_3 and evaporated again. During this step, silicon Si and other volatile species are lost, and residual elements are concentrated. Incipient dry residues were re-dissolved in 3 mL of 1 N HNO_3 at 195 °C for 12 h, and after cooling to room temperature, made up to 80.0 ± 0.005 g with dilute HNO_3 at ~pH 2 for analysis in an Agilent 7500A ICP-MS instrument. Lower limits of detection (LLD) are listed per trace element species in a separate column in Table 3.

Optical petrography

The Chu Lai intrusion mainly consists of granitic gneiss, Bt-Grt gneiss and two mica gneiss (Fig. 3b, c). Its mineral content consists of plagioclase (25-30 vol%), K-feldspar (15-20 vol%), microcline (10-15 vol%), quartz (30-35 vol%) and

Table 2 Main element oxide contents in weight percent (wt%) of samples from the Chu Lai granite, by XRF. LOI determined gravimetrically on a separate aliquot. $Fe_2O_3^T$ represents total iron. Sample locations indicated in Fig.2. Further explanation in text

Sample (V17##)	LLD	22	23	24	25	27	28	29	30
SiO_2	0.05	74.8	74.5	71.8	73.9	70.2	74.2	71.5	73.5
TiO_2	0.01	0.16	0.15	0.20	0.29	0.39	0.16	0.35	0.23
Al_2O_3	0.05	13.5	13.7	13.0	12.9	14.5	13.7	14.2	13.9
$Fe_2O_3^T$	0.01	1.34	1.27	2.78	2.62	3.71	1.63	2.83	1.80
MnO	0.01	0.03	0.04	0.03	0.03	0.09	0.05	0.06	0.04
MgO	0.01	0.34	0.25	0.45	0.39	0.67	0.35	0.96	0.37
CaO	0.01	0.93	0.91	1.16	0.56	2.08	1.82	2.93	1.18
Na_2O	0.01	2.51	2.70	3.78	1.96	4.24	3.06	2.66	2.56
K_2O	0.01	6.13	5.59	5.56	6.22	3.02	4.52	3.82	6.18
P_2O_5	0.01	0.08	0.08	0.06	0.08	0.13	0.04	0.08	0.05
LOI	0.01	0.38	0.52	0.46	0.65	0.02	0.01	0.01	0.01
TOTAL		100.17	99.75	99.24	99.56	99.07	99.47	99.31	99.82
Calculated parameters									
K_2O/Na_2O		2.44	2.07	1.47	3.17	0.71	1.48	1.44	2.41
A/CNK*		1.08	1.13	0.91	1.17	1.03	1.03	1.02	1.06
A/NK**		1.25	1.31	1.06	1.29	1.41	1.38	1.66	1.27

*value calculated as: molar $Al_2O_3/(CaO + Na_2O + K_2O)$

**value calculated as: molar $Al_2O_3/(Na_2O + K_2O)$

biotite (~5 vol%) (Fig. 3e). Two mica gneiss is fine-grained and is composed of plagioclase (25-30 vol%), K-feldspar (25-30 vol%), quartz (30-35 vol%), biotite (~3 vol%) and muscovite (~2 vol%). Bt-Grt gneiss is light grey and medium-grained and weakly foliated (Fig. 3d). Its major minerals include plagioclase (28-35 vol%), K-feldspar (25-30 vol%) quartz (20-30 vol%), biotite (3-5 vol%) and garnet (1-5 vol%) (Fig. 3f). Accessory minerals are apatite, zircon, and ilmenite. Garnet and tourmaline are occasionally found. Perthitic structures were commonly observed in K-feldspar core. Plagioclase, biotite, and muscovite are prismatic, but quartz has a rounded shape. Thin section petrography in transmitted light reveals that the Chu Lai pluton contains alumina-rich minerals like muscovite and garnet (Fig. 3f).

Results

Whole-rock main and trace element contents

Both major and trace element compositions of the samples taken from the Chu Lai pluton are shown in Tables 2 and 3. The Bt-Grt gneiss in the Chu Lai intrusion is characterized by high SiO_2 (71.8–75.3 wt%), $Na_2O + K_2O$ (8.18–9.34 wt%), K_2O (5.56–6.22 wt%) contents with K_2O/Na_2O ratios from 1.47 to 3.17. In addition, it indicates low contents of TiO_2 (0.15–0.29 wt%), $Fe_2O_3^t$ (1.27–2.78 wt%), CaO (0.56–1.18 wt%) and MgO (0.25–0.45 wt%). The granitic gneiss in the Chu Lai intrusion also shows high SiO_2 (70.2–74.2 wt%), $Na_2O + K_2O$ (6.48–7.58 wt%), K_2O (3.02–4.52 wt%) contents with K_2O/Na_2O ratios from 0.71 to 1.48. Moreover, it displays low contents of TiO_2 (0.16–0.39 wt%), $Fe_2O_3^t$ (1.63–3.71 wt%), CaO (1.82–2.93) and MgO (0.35–0.96 wt%). The Bt-Grt gneiss contains higher SiO_2, $Na_2O + K_2O$, and K_2O values than granitic gneiss, however, the Bt-Grt gneiss shows lower TiO_2, $Fe_2O_3^t$, CaO and MgO contents than granitic gneiss. The difference in petrography and geochemistry of the Chu Lai granite was thought to be influenced by post-metamorphic events (344 Ma and 253 Ma) recorded on the Chu Lai intrusion. Based on the SiO_2 vs $K_2O + Na_2O$ diagram, the Chu Lai samples fall into the granite field (Fig. 4a). Their A/CNK and A/NK ratios are 0.91–1.17 and 1.06–1.66, respectively (Fig. 4b). On a SiO_2 vs. K_2O diagram (Fig. 4c), they display a trend of high K-shoshonitic behavior. Finally, petrographic classification suggests that the Chu Lai granite is a S-type granite (Fig. 4d).

In a chondrite-normalized spider diagram (Sun and McDonough 1989), nine samples from the Chu Lai granite show enrichment of LREE, strong negative Eu anomalies ($Eu/Eu^* = 0.21–0.71$), LREE/HREE ratios of 4.55–9.80, and $(La/Yb)_N$ ratios of 3.24–12.44 (Fig. 5a). They all show negative anomalies of Ba, Nb, Ta, Sr, and Ti but positive anomalies of Rb, Th, U, K, and Pb (Fig. 5b). The positive anomalies of Rb, Th, and K as well as negative anomalies of Sr, P, and Ti are evidence of partial melting of an ancient crust (He et al. 2016). Major element compositions imply that the Chu Lai granite is produced by partial melting of greywacke and pelite (Fig. 6).

Table 3 Trace element and REE contents in parts per million (ppm; $\mu g \cdot g^{-1}$) of samples from the Chu Lai granite, by ICP-MS. Sample locations indicated in Fig.2. Further explanation in text

Sample (V17##)	LLD	22	23	24	25	26	27	28	29	30
Trace elements										
Sc	0.01	2.58	2.73	2.62	2.76	2.54	7.71	4.27	7.21	6.12
V	0.01	6.09	4.84	5.89	6.17	5.23	18.71	10.42	44.31	12.02
Cr	0.01	5.53	4.28	5.42	4.76	5.12	5.53	2.61	10.46	3.51
Ni	0.01	1.57	3.03	2.12	2.67	3.01	4.80	4.31	8.12	7.16
Cu	0.05	16.50	20.30	18.70	19.20	17.60	6.21	2.62	4.53	1.85
Zn	0.05	20.10	24.40	21.20	22.70	24.20	57.01	28.05	30.56	31.25
Ga	0.05	17.70	15.80	16.50	15.50	17.60	17.20	13.41	15.34	16.03
Rb	1.00	274	265	268	272	262	113	174	166	311
Sr	0.50	43.3	56.0	46.5	52.6	55.8	145	171.7	218.2	69.9
Zr	1.00	119	128	124	129	116	243	97	115	145
Nb	0.10	20.6	14.5	16.6	17.8	19.3	15.80	8.5	10.2	16.2
Cs	0.01	7.96	9.85	8.17	8.32	9.67	3.88	3.99	4.68	4.89
Ba	1.00	216	252	246	232	256	619	885	553	284
Hf	0.01	3.68	3.98	3.58	3.72	3.64	6.90	3.46	3.87	5.06
Ta	0.01	1.58	1.35	1.62	1.46	1.55	1.68	1.31	1.36	2.67
Pb	0.05	47.10	50.20	48.20	49.70	46.90	17.97	31.49	16.52	37.29
Th	0.05	36.40	35.20	35.80	37.10	36.20	13.90	15.52	16.53	32.72
U	0.10	12.1	10.3	11.1	12.8	10.7	3.6	3.6	2.9	7.8
Rare earth elements + yttrium (REE + Y)										
La	0.10	44.7	43.8	44.9	42.3	46.5	32.98	20.9	23.6	88.8
Ce	0.10	100.7	98.8	97.6	95.9	101.8	65.91	41.1	47.7	166.9
Pr	0.02	10.60	10.40	9.70	11.20	10.70	7.78	4.60	4.80	19.35
Nd	0.30	38.0	37.4	39.3	36.8	37.6	30.3	17.2	17.0	74.5
Sm	0.05	8.58	8.51	9.15	8.26	8.67	6.21	3.41	7.56	13.24
Eu	0.02	0.56	0.67	0.72	0.53	0.62	1.39	0.78	0.76	0.93
Gd	0.05	7.80	8.17	6.90	7.31	8.26	6.04	3.30	4.56	11.39
Tb	0.01	1.25	1.41	1.27	1.65	1.38	1.02	0.55	1.28	1.79
Dy	0.05	7.19	8.87	8.12	7.56	7.84	6.13	3.40	4.76	9.93
Ho	0.02	1.40	1.93	1.6	1.86	1.78	1.25	0.71	1.78	1.88
Er	0.03	3.74	5.58	4.87	4.76	5.21	3.77	2.16	3.76	5.44
Tm	0.01	0.57	0.89	0.76	0.82	0.65	0.58	0.32	0.57	0.81
Yb	0.05	3.89	6.22	4.32	5.23	6.11	3.85	2.17	5.23	5.12
Lu	0.01	0.56	0.89	0.62	0.67	0.78	0.60	0.34	0.36	0.74
Y	0.50	43.5	63.0	56.8	62.0	58.6	36.0	22.0	19.5	55.5
Calculated element ratios										
$(La/Yb)_N$		8.24	5.05	7.46	5.80	5.46	6.14	6.91	3.24	12.44
$(Tb/Yb)_N$		1.46	1.03	1.34	1.43	1.03	1.20	1.15	1.11	1.59
Eu/Eu*		0.21	0.25	0.28	0.21	0.23	0.70	0.71	0.40	0.23

Zircon U-Pb age

The CL images of zircon in the Chu Lai granite are presented in Fig. 7. Most of the zircons are colorless and transparent to pale yellow and indicate clear oscillatory zoning in CL images. The results of LA-ICP-MS U-Pb isotopic analyses are graphically shown in Fig. 7 and displayed in Table S1.

Four zircon U-Pb samples (V1722, V1723, V1724, and V1726) represent the Chu Lai granite as shown in Table S1. These zircons were virtually colorless and transparent (Fig. 7). First, V1722 lacks a zonal structure (Fig. 7a) with average Th/U ratio = 0.70 (>0.1), indicating magmatic origin (Wu and Zheng 2004). Thirteen out of twenty zircon grains are closely characterized by a concordant U-Pb age of 445 ± 7 Ma (n =

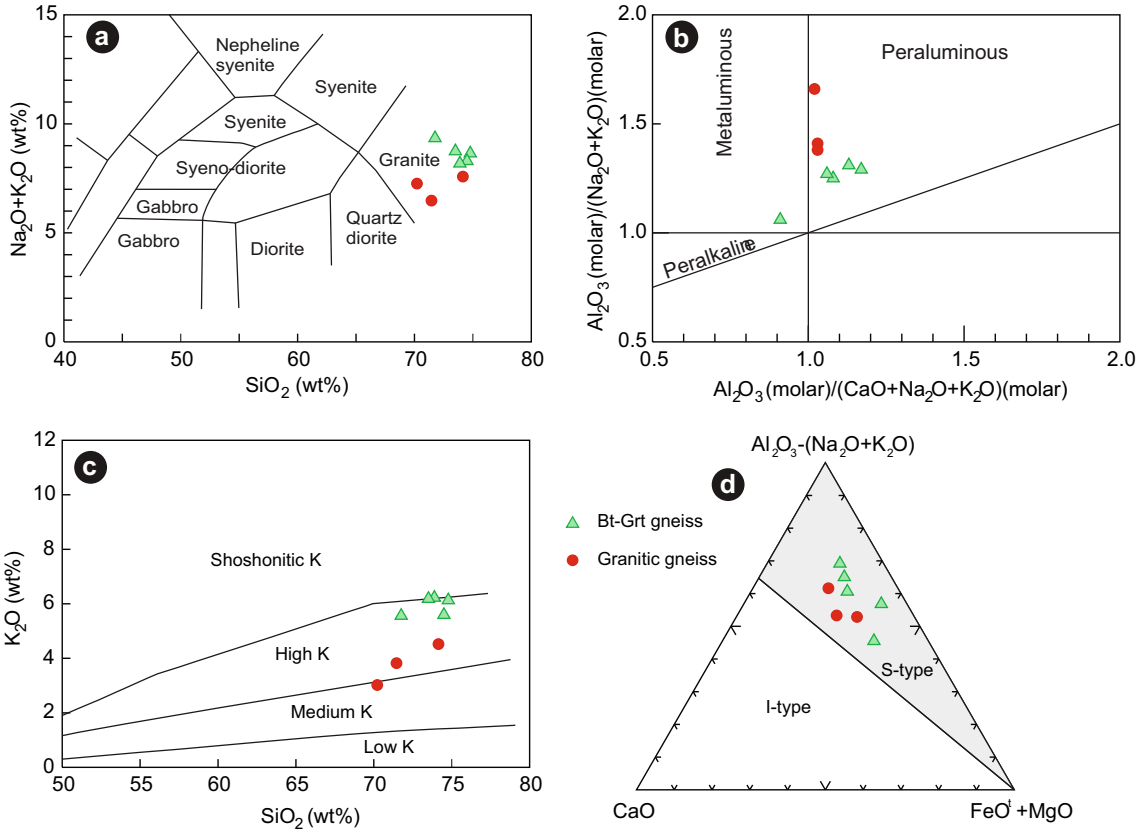

Fig. 4 a SiO_2-($Na_2O + K_2O$) (Wilson 1989). b molar ratio of Al_2O_3/($CaO + Na_2O + K_2O$) and Al_2O_3/($Na_2O + K_2O$) (Frost et al. 2001). c K_2O-SiO_2 (Peccerillo and Taylor 1976). d discrimination diagram of type granite (Wang et al. 2018)

13, MSWD = 0.78; Fig. 8a), interpreted as crystallization age of V1722. The seven remaining zircon grains show Neoarchean (2755 Ma), Mesoproterozoic (1565 Ma, 1250 Ma, 1174 Ma, and 1106 Ma) and Neoproterozoic (717 Ma and 704 Ma) U-Pb age. These ages are concentrated particularly in the core portion of zircons, suggesting that they reflect relics of Precambrian crust. Sample V1723 shows zircons with oscillatory zoning (Fig. 7b) with an average Th/U ratio = 0.37 (>0.1), typical for magmatic origin (Wu and Zheng 2004). Ten out of 17 zircon grains have a concordant U-Pb age of 453 ± 16 Ma ($n = 10$, MSWD = 3.8; Fig. 8b), interpreted as crystallization age of V1723. The five remaining zircon grains indicate Paleoproterozoic (1928 Ma and 1856 Ma), Mesoproterozoic (1215 Ma) and Neoproterozoic (844 Ma and 831 Ma) U-Pb age. As in V1722, these older ages were inherited from the Precambrian crust. Two remaining zircon grains show a Carboniferous (344 Ma; Th/U ratio = 0.002 < 0.1) and late Permian (253 Ma; Th/U ratio = 0.056 < 0.1) U-Pb age, indicating possible metamorphic events. Sample V1724 contains zircons with a zonal structure (Fig.

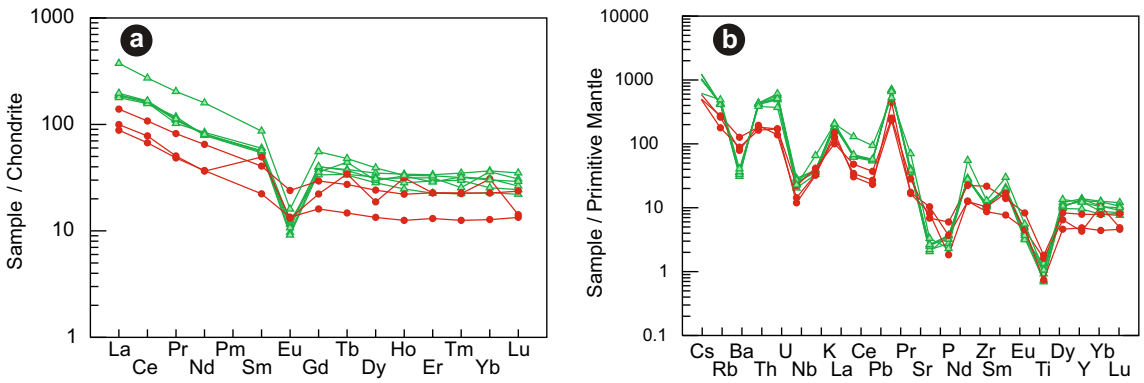

Fig. 5 Primitive mantle-normalized trace element patterns as well as chondrite-normalized REE patterns for the Chu Lai granite rocks (Sun and McDonough 1989)

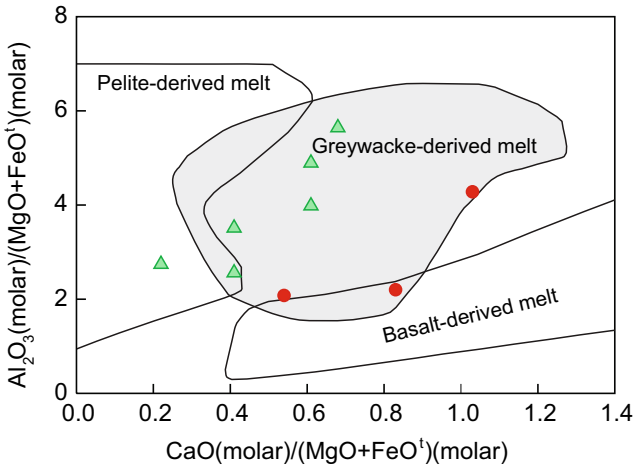

Fig. 6 Molar ratio of $Al_2O_3/(MgO + FeO^t)$ and $CaO/(MgO + FeO^t)$ (Altherr et al. 2000)

7c) with average Th/U ratio of 0.80 (>0.1), indicating magmatic origin (Wu and Zheng 2004). Nineteen zircon grains yield a concordant U-Pb age of 454 ± 6 Ma ($n = 19$, MSWD = 0.82; Fig. 8c), displaying the crystallization age of V1724. An oscillatory zoning was observed in zircons from sample V1726 (Fig. 7d) with average Th/U ratio = 0.51 (>0.1), indicating magmatic origin (Wu and Zheng 2004). Sixteen zircon grains give a concordant U-Pb age of 454 ± 14 Ma ($n = 16$, MSWD = 0.08; Fig. 8d), interpreted as crystallization age of V1726.

Nd and Hf isotopes

The whole-rock Sm-Nd isotopic composition varies from $(^{143}Nd/^{144}Nd)_i = 0.511643$ to 0.511832 and for $^{147}Sm/^{144}Nd$ from 0.1285 to 0.1232 (Table S2). We used the inferred intrusion age of 454 Ma to calculated the initial Nd isotopic compositions. Four samples from the Chu Lai granite exhibit initial ε_{Nd} values from −5.8 to −8.3, with T_{DM2} model ages of 1.67–1.89 Ga. The Nd isotopic characteristics (Barbarin, 1999) points to partial melting of an ancient crustal source.

Zircon grains from three Chu Lai samples (V1722, V1723, and V1726) were analyzed for Lu-Hf isotopic compositions (Table S3 and Fig. 9). For V1722, twenty zircon grains display negative values of $\varepsilon_{Hf}(t)$ from −9.6 to −1.8 with a mean of −7.3 ± 1.1 (MSWD = 0.46). Estimated T_{DM2} model ages range from 1547 Ma to 2039 Ma with a mean of 1895 ± 50 Ma (MSWD = 18). They also show $^{176}Lu/^{177}Hf$ ratios of 0.000447–0.001311 and $^{176}Hf/^{177}Hf$ ratios of 0.282234–0.282450. For V1723, 18 zircon grains show values of $\varepsilon_{Hf}(t)$ range from −16.1 to −1.0 (Mean = −6.7 ± 1.4, MSWD = 1.3) and T_{DM2} model ages from 1503 Ma to 2449 Ma (Mean = 1864 ± 91, MSWD = 53). The $^{176}Lu/^{177}Hf$ ratios range from 0.000606 to 0.005934 and $^{176}Hf/^{177}Hf$ from 0.282055 to 0.282514. For V1726, twenty-six zircon grains yielded negative $\varepsilon_{Hf}(t)$ values (−16.7 to −2.7) (Mean value = −7.07 ± 1.4, MSWD = 1.3) and T_{DM2} model ages from 1503 Ma to 2449 Ma (Mean value = 1864 ± 91, MSWD = 53). $^{176}Lu/^{177}Hf$ ratios range from 0.000484 to 0.001401 and $^{176}Hf/^{177}Hf$ from 0.282025 to 0.282428.

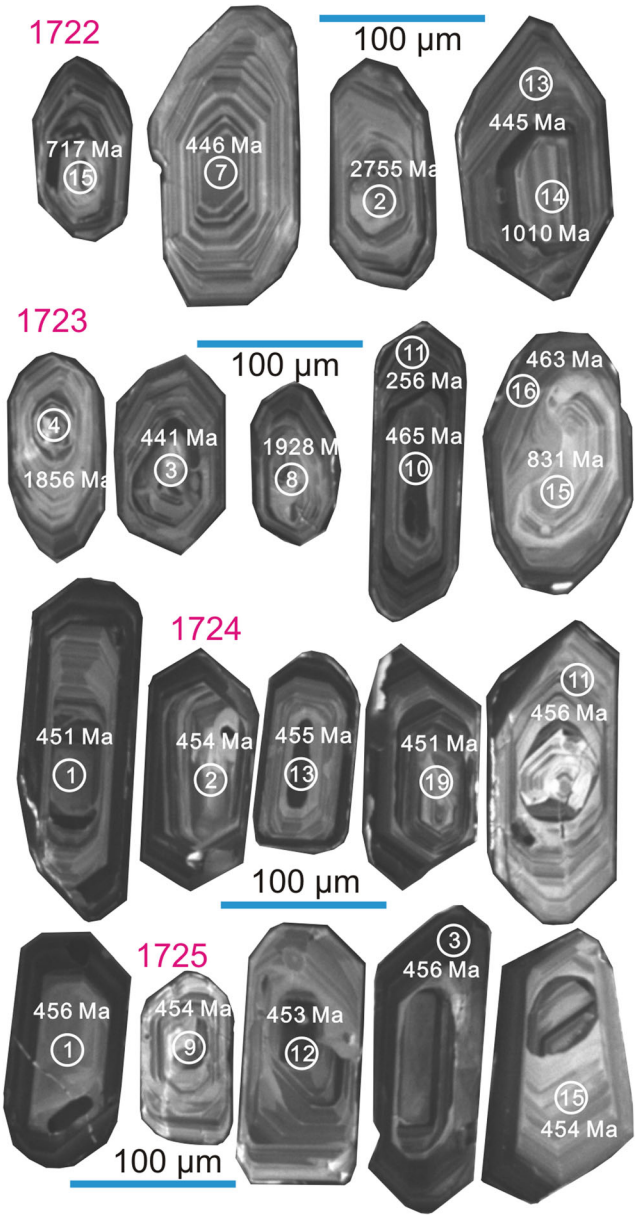

Fig. 7 Cathodoluminescence images of the Chu Lai zircon

Discussion

The emplacement age of the Chu Lai granite

The Chu Lai granitic pluton intruded into the Kham Duc Complex which is considered to have Proterozoic age. Cambrian-Silurian sedimentary rocks unconformably cover the Chu Lai granite. According to field observations, the

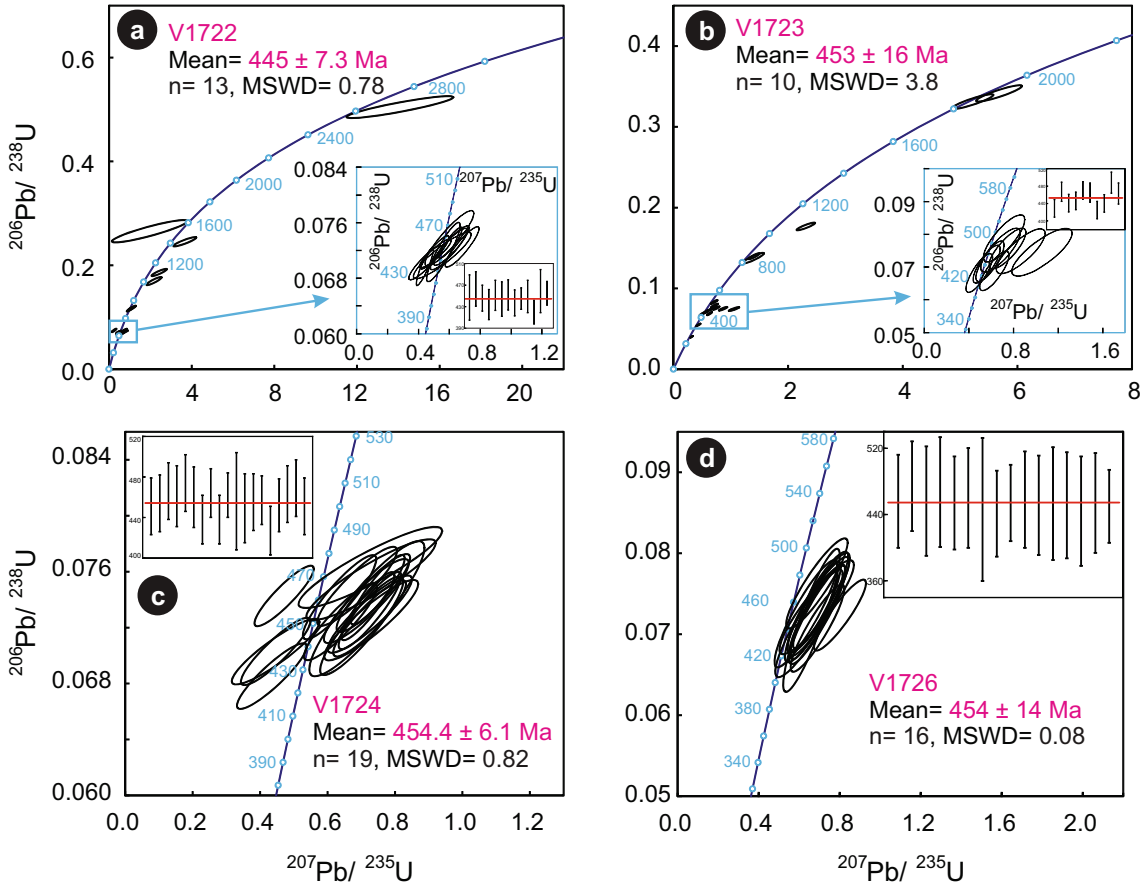

Fig. 8 Zircon LA-ICP-MS U-Pb results for the Chu Lai rocks

emplacement age of the Chu Lai granite is likely to be Late Proterozoic (Thuc and Trung, 1995). Radiometric age determination using the whole rock Rb-Sr method indicates an age of 530 Ma (Hurley and Fairbairn, 1972) and 515 Ma (Tam 2008). In both publications no detailed data are given. In this study, we used LA-ICP-MS U-Pb zircon analyses for the determination of the age of crystallization. The obtained age vary between 445 ± 7 Ma to 454 ± 6 Ma, clearly indicating the granite emplacement age during the Ordovician-Silurian. Our U-Pb dating of zircons, along with the previously reported 426–423 Ma Dai Loc granite (Hieu et al. 2016), 429.8 Ma schist (Tran et al. 2014), 450–422 Ma Kan Nak gneiss and 462–429 Ma Ngoc Linh gneiss (Nakano et al. 2013), 468–444 Ma Song Bien granulite (Roger et al. 2007), provide evidence for Ordovician-Silurian magmatism in the Kontum massif.

The origin of the Chu Lai granite

The Chu Lai granite is characterized by A/CNK ratios of 0.91–1.17, with an average of 1.06. Trace element composition indicates that the Chu Lai granite is enriched in Rb, Th, U, and Pb, but depleted in Ba, Nb, Ta, Sr, Ti, and Eu. Geochemically, the Chu Lai granite most likely originates from partially molten crustal material according to Wang et al. (2018) and Altherr et al. (2000) (Figs. 4 and 6). The common presence of Al-rich minerals (muscovite, garnet and tourmaline) suggests that the Chu Lai granite is a S-type granite (Wang et al. 2018). In addition, U-Pb ages determined from inherited zircon cores from sample V1722 and V1723 reflect the contribution of Precambrian crustal components in the Chu Lai granite (Fig. 6). Indeed, zircon ε_{Hf} values of −16.7 to −1, and whole rock ε_{Nd} values of −8.3 to −5.8 from the Chu Lai granite indicate ancient crustal material (Fig. 9a–e; Table S2 and S3). The Hf model ages (T_{DM2}) obtained from single zircon grains range from 1.50 to 2.49 Ga and Nd model ages (T_{DM2}) on whole rocks vary from 1.67 to 1.89 Ga and (Fig. 9b–f). Thus, the Chu Lai granite was produced by partial melting of Proterozoic rocks during the Ordovician-Silurian period.

Tectonic implications

Recent progress in geochemistry and petrology using U-Pb zircon isotopic ages allows to constrain the evolution of the Kontum massif. It is evidenced that there were at least two magmatic episodes occurring in the Phanerozoic. In specific, a first phase of tectonic activity is seen in intensive magmatism

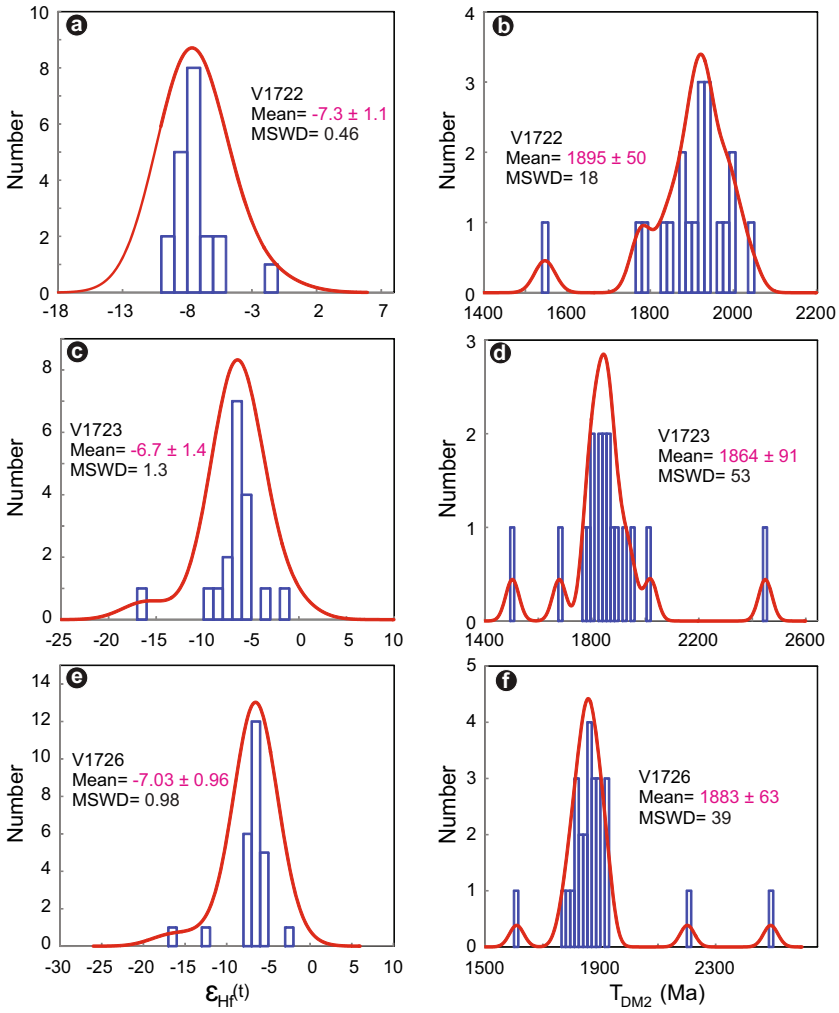

Fig. 9 Histograms of zircon $\varepsilon_{Hf}(t)$ values and zircon Hf-isotope crust model age (T_{DM2}) of the Chu Lai rocks

and associated metamorphic overprint that occurred in Ordovician-Silurian time (470–427 Ma; Hieu et al. 2016). This episode of Paleozoic tectonic activity in the Kontum massif was established with the help of modern high-resolution U/Pb age dating in combination with field evidence (Carter et al. 2001; Nam et al. 2004; Vuong et al. 2004; Luat, Hieu and Thanh, 2012; Hieu et al. 2016). The second phase of tectonic activity in the Kontum massif occurred 250–260 Ma. In particular, the later tectonic event is mainly observed in the Kan Nack granulite facies and Ngoc Linh amphibolite facies units (Carter et al. 2001; Nagy et al. 2001; Nam et al. 2001; Nakano et al. 2007) as recorded by rejuvenated Sm-Nd ages of 240 ± 16 Ma and 247 ± 11 Ma.

Whole rock Nd T_{DM2} model ages indicate 1.67–1.89 Ga and zircon Hf T_{DM2} model ages display 1.6 Ga to 2.4 Ga. The Nd and Hf isotopic model ages are similar to those of the South China basement rocks (e.g., Wang et al. 2014). In Fig. 10 and Table S4, ε_{Hf} values and T_{DM2} ages of the Indochina block are similar to those of the Yangtze block (Zhang et al. 2010; Wang et al. 2011; Chu et al. 2012; Zhang et al. 2012; Zhou et al. 2017), but differ to the Cathaysia block. Comparison of ε_{Hf} and crystallization age results indicates that Indochina was quite close to the Yangtze block/South China block in the Ordovician-Silurian time (Fig. 11). The Chu Lai granitic plutons contain inherited zircons of Precambrian age (2.7 Ga, 1.9 Ga, 1.8 Ga, 1.5 Ga, 1.2 Ga, 1.1 Ga, 844 Ma, 831 Ma, 717 Ma, and 704 Ma), which corresponds to common magmatic activities documented in the South China block (Chen et al. 2003; Yu et al. 2008; Shu et al., 2011a, b; Wang et al., 2013a; Wang et al. 2014). According to isotopic analysis, it is possible that the Kontum massif had a close spatial affinity to the South China block in the past.

The tectonic cause of the Chu Lai granite formation at 445–454 Ma remains a matter of controversy. There are several tectonic models to explain the Ordovician-Silurian event in the Kontum massif such as a subduction-related setting along an active continental margin (Tri and Khuc 2011; Hieu et al. 2016), island arc (Nagy et al. 2001), intracontinental collision within the South China block (Zhu and Long 1997; Quoc and Luong 1986; Xiang and Shu, 2010; Zhang et al. 2012; Wang et al., 2013b; Shu et al. 2014, 2015), and collision between the South China and Indochina blocks (Usuki et al. 2009). On the other hand, Wang et al. (2007) reported that intracontinental

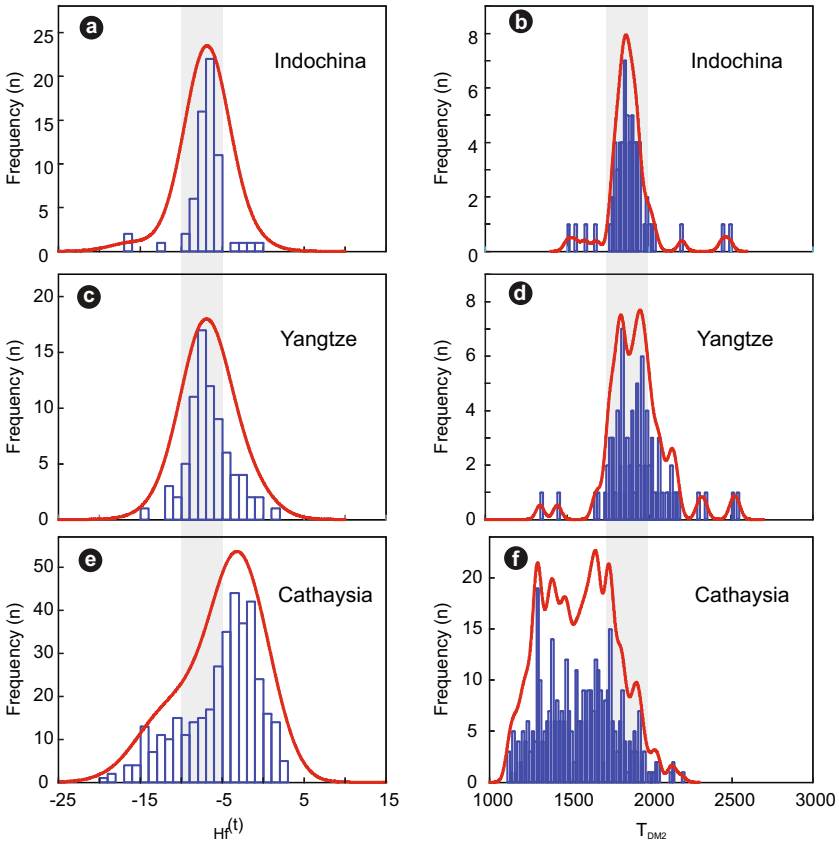

Fig. 10 Histogram of initial ε_{Hf} values and Hf model ages of zircons from the Indochina, Yangtze and Cathaysia. Comparison data is derived from Zhang et al. 2010; Wang et al. 2011; Chu et al. 2012; Zhang et al. 2012; Zhou et al. 2017 and this study

collision between the Yangtze block and Cathaysia block caused the Caledonian tectonothermal event (450–400 Ma). This study in combination with previously published results indicates that in Ordovician–Silurian times the Kontum massif endorses the existence of Paleotethyan ocean crust during 480–450 Ma. The Paleothetys ocean crust subducted beneath the Indochina continental crust, forming I-type granite of Ben Giang complex (Dien Binh complex) which is located in the northern Tam Ky-Phuoc Son fault (Tam Ky-Phuoc Son ophiolite) and is widely distributed in Kontum massif, Central Vietnam. (Tran et al. 2014). Then, the development of an intracontinental orogen formed the Chu Lai S-type granite in the Truong Son belt, Kontum massif (Nakano et al. 2013) (Fig. 12).

Conclusions

Integrated petrological studies, geochemistry, zircon U-Pb ages and Nd-Hf isotopes of the Chu Lai granite from the Kontum massif, central Vietnam allow us to provide the following major conclusions: (1) The Chu Lai granite mainly consists of granitic gneiss, Bt-Grt gneiss and two mica gneiss with Al-rich minerals. Geochemically, it is a high K-shoshonitic rock with depletion of Ba, Nb, Ta, Sr, Ti, and Eu and enrichment of Rb, Th, U, and Pb. The zircon εHf values of the Chu Lai granite range from −16.7 to −1 and Hf model ages (TDM2) from 1.50 to 2.49 Ga as well as whole-rock εNd values vary from −8.3 to −5.8 and Nd model ages (TDM2) from 1.67 to 1.89 Ga, respectively; (2) The Chu Lai granite

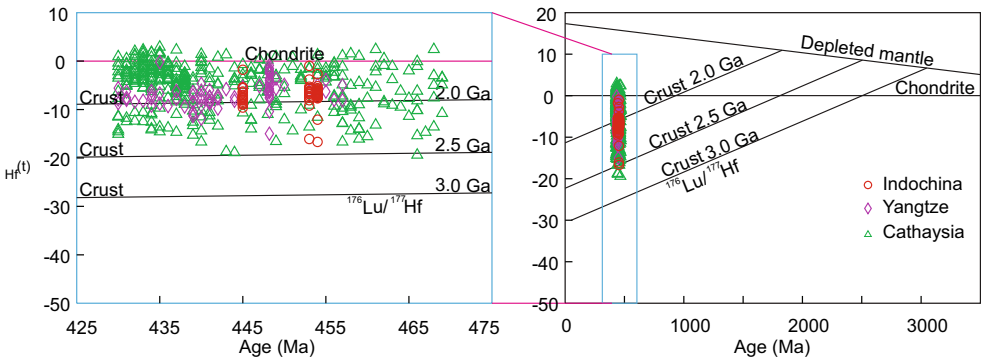

Fig. 11 Initial ε_{Hf} values and ages of zircons from the Indochina, Cathaysia, and Yangtze. Comparison data is derived from Zhang et al. (2010); Wang et al. (2011); Chu et al. (2012); Zhang et al. (2012); Zhou et al. (2017) and this study

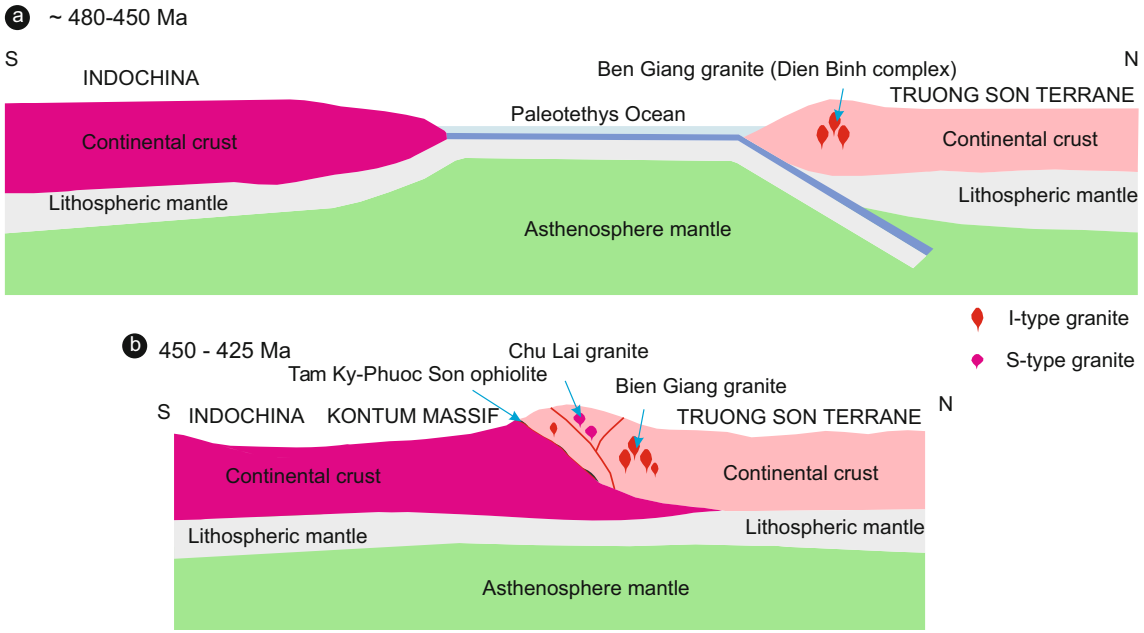

Fig. 12 Tectonic setting for the Chu Lai granite and others of Ordovician–Silurian in Indochina (modified after Nakano et al. 2013)

was emplaced during the Ordovician-Silurian at 445–454 Ma, providing evidence for Ordovician-Silurian magmatism in the Kontum massif; (3) The Chu Lai granite displays typical S-type granite characteristics and must have been the product of partial melting of Proterozoic basement materials; (4) The development of an intracontinental orogen formed the Chu Lai S-type granite in the Truong Son belt, Kontum massif. The Kontum massif had a close spatial affinity to the South China block in the past. Indochina block was quite close to the Yangtze block/South China block in the Ordovician-Silurian time.

Acknowledgments This study was supported by the Vietnam Academy of Science and Technology (VAST) [Project code BSTMV.06/14-16, VAST05.02/19-20 and TN17/T06] and Project code No.105.05-2010.01. Thanks are due to Prof. Fukun Chen and Wang W for assistance during chemical and isotopic analyses. The manuscript benefits greatly from the constructive and helpful review from Dr. N Nakano and the authors thank the editorial handling by Dr. Christoph Hauzenberger and Prof. Maarten Broekmans.

References

Altherr R, Holl A, Hegner E, Langer C, Kreuzer H (2000) High-potassium, calc-alkaline I-type plutonism in the European Variscides: northern Vosges (France) and northern Schwarzwald (Germany). Lithos 50:51–73

Barbarin B (1999) A review of the relationships between granitoid types, their origins and their geodynamic environments. Lithos 46:605–626

Carter A, Roques D, Bristow C, Kinny P (2001) Understanding Mesozoic accretion in Southeast Asia: significance of Triassic thermotectonism (Indosinian orogeny) in Vietnam. Geology 29: 211–214

Chen F, Siebel W, Guo J, Cong B, Satir M (2003) Late Proterozoic magmatism and metamorphism recorded in gneisses from the Dabie high-pressure metamorphic zone, eastern China: evidence from zircon U–Pb geochronology. Precambrian Res 120:131–148

Chen F, Li XH, Wang XL, Li QL, Siebel W (2007) Zircon age and Nd-Hf isotopic composition of the Yunnan Tethyan belt, southwestern China. Int J Earth Sci 96:1179–1194

Chen F, Hegner E, Todt W (2000) Zircon ages, Nd isotopic and chemical compositions of orthogneisses from the Black Forest, Germany - evidence for a Cambrian magmatic arc. Int J Earth Sci 88:791–802

Chu Y, Lin W, Faure M, Wang Q, Ji W (2012) Phanerozoic tectonothermal events of the Xuefengshan Belt, central South China: implications from UPb age and LuHf determinations of granites. Lithos 150:243–255

Frost CD, Bell JM, Frost BR, Chamberlain KR (2001) Crustal growth by magmatic underplating: isotopic evidence from the northern Sherman batholith. Geology 29:515–518

He D, Dong Y, Zhang F, Yang Z, Sun S, Cheng B, Zhou B, Liu X (2016) The 1.0 Ga S–type granite in the east Kunlun Orogen, northern Tibetan plateau: implications for the Meso–to Neoproterozoic tectonic evolution. J Asian Earth Sci 130:46–59

Hieu PT, Chen FK, Wang W, Nguyen TBT, Bui MT, Nguyen QL (2009) Zircon U-Pb ages and Hf isotopic composition of the Posen granite in Northwest Vietnam. Acta Petrol Sin 25:3141–3152

Hieu PT, Yang YZ, Binh DQ, Nguyen TBT, Dung LT, Chen F (2015) Late Permian to early Triassic crustal evolution of the Kontum massif, Central Vietnam: zircon U–Pb ages and geochemical and Nd–Hf isotopic composition of the Hai Van granitoid complex. Int Geo Rev 57:1877–1888

Hieu PT, Dung NT, Nguyen TBT, Minh NT, Minh P (2016) U–Pb ages and Hf isotopic composition of zircon and bulk rock geochemistry of the Dai Loc granitoid complex in Kontum massif: implications for early Paleozoic crustal evolution in Central Vietnam. Miner Petrol Sci 111:326–336

Hieu PT, Li SQ, Yu Y, Thanh NX, Dung LT, Tu VL, Siebel W, Chen F (2017) Stages of late Paleozoic to early Mesozoic magmatism in the song Ma belt, NW Vietnam: evidence from zircon U–Pb geochronology and Hf isotope composition. Int J Earth Sci 106:855–874

Hoa TT, Anh TT, Phuong NT, Dung PT, Anh TV, Izokh AE, Borisenko AS, Lan CY, Chung SL, Lo CH (2008) Permo-Triassic intermediate–felsic magmatism of the Truong son belt, eastern margin of Indochina. Compt Rendus Geosci 340:112–126

Humphries DW (1992) The preparation of thin sections of rocks, minerals and ceramics. Royal Microscopical Society, Oxford Science Publications, Microscopy Handbooks 24: pp 83

Hurley PM, Fairbairn HW (1972) Sb-Sr ages in Vietnam: 530 M.y. event. Bull. Geol Soc Am Bull 83:3523–3528

Hutchison CS 1989. Geological evolution of south-East Asia. Oxford, Oxford Science Publications, 368

Iizuka T, Yamaguchi T, Itano K, Hibiya Y, Suzuki K (2017) What Hf isotopes in zircon tell us about crust–mantle evolution. Lithos 274: 304–327

Lan CY, Chung SL, Jiun-San Shen J, Lo CH, Wang PL, Hoa TT, Thanh HH, Mertzman SA (2000) Geochemical and Sr–Nd isotopic characteristics of granitic rocks from northern Vietnam. J Asian Earth Sci 18:267–280

Liu Y, Hu Z, Gao S, Günther D, Xu J, Gao C, Chen H (2008) In situ analysis of major and trace elements of anhydrous minerals by LA-ICP-MS without applying an internal standard. Chem Geo 257:34–43

Liu Y, Gao S, Hu Z, Gao C, Zong K, Wang D (2010) Continental and oceanic crust recycling-induced melt–peridotite interactions in the trans-North China Orogen: U–Pb dating, Hf isotopes and trace elements in zircons from mantle xenoliths. J Petrol 51:537–571

Luat NQ, Hieu PT, Thanh NT (2012) U-Pb zircon isotopic age and Hf zircon isotopic composition of a bung gabbrodiorite in the Đắk Krông – a Lưới area. J Geo 329, 19–29 (In Vietnamese with English abstract)

Metcalfe I (2013) Gondwana dispersion and Asian accretion: tectonic and palaeogeographic evolution of eastern Tethys. J Asian Earth Sci 66: 1–33

Nagy EA, Maluski H, Lepvrier C, Schaer U, Thi PT, Leyreloup A, Thich VV (2001) Geodynamic significance of the Kontum massif in Central Vietnam: composite $^{40}Ar/^{39}Ar$ and U-Pb ages from Paleozoic to Triassic. J Geol 109:755–770

Nakano N, Osanai Y, Owada M, Nam TN, Toyoshima T, Binh P, Tsunogae T, Kagami H (2007) Geologic and metamorphic evolution of the basement complexes in the Kontum massif, Central Vietnam. Gondwana Res 12:438–453

Nakano N, Osanai Y, Owada M, Nam TN, Charusiri P, Khamphavong K (2013) Tectonic evolution of high-grade metamorphic terranes in Central Vietnam: constraints from large-scale monazite geochronology. J Asian Earth Sci 73:520–539

Nam TN, Sano Y, Terada K, Toriumi M, Van Quynh P (2001) First SHRIMP U–Pb zircon dating of granulites from the Kontum massif (Vietnam) and tectonothermal implications. J Asian Earth Sci 19: 77–84

Nam TN, Osanai Y, Nakano N, Tham HH (2004) Permo-Triassic ultra-high-temperature metamorphism and continental collision in the Kon Tum massif. J Geo 285:1–8 (in Vietnamese with English abstract)

Osanai Y, Nakano N, Owada M, Nam TN, Toyoshima T, Tsunogae T, Binh P (2004) Permo-Triassic ultrahigh-temperature metamorphism in the Kontum massif, Central Vietnam. Miner Petrol Sci 99:225–241

Owada M, Osanai Y, Nakano N, Matsushita T, Nam TN, Tsunogae T, Toyoshima T, Binh P, Kagami H (2007) Crustal anatexis and formation of two types of granitic magmas in the Kontum massif, Central Vietnam: implications for magma processes in collision zones. Gondwana Res 12:428–437

Peccerillo A, Taylor SR (1976) Geochemistry of Eocene calc-alkaline volcanic rocks from the Kastamonu area, northern Turkey. Contrib Mineral Petr 58:63–81

Quoc NK, Luong PD (1986) The great stages of volcanic activities in Vietnam. Proc. 1st Conf. Geol. Indochina, Hanoi, 1: 179–190

Roger F, Maluski H, Leyreloup A, Lepvrier C, Thi PT (2007) U–Pb dating of high temperature metamorphic episodes in the Kon Tum massif (Vietnam). J Asian Earth Sci 30:565–572

Scherer E, Munker C, Mezger K (2001) Calibration of the lutetium-hafnium clock. Science 293:683–687

Shi MF, Lin FC, Fan WY, Deng Q, Cong F, Tran MD, Zhu HP, Wang H (2015) Zircon U–Pb ages and geochemistry of granitoids in the Truong son terrane, Vietnam: tectonic and metallogenic implications. J Asian Earth Sci 101:101–120

Shu LS, Deng XL, Zhu WB, Ma DS, Xiao WJ (2011a) Precambrian tectonic evolution of the Tarim block, NW China: new geochronological insights from the Quruqtagh domain. J Asian Earth Sci 42: 774–790

Shu LS, Faure M, Yu JH, Jahn BM (2011b) Geochronological and geochemical features of the Cathaysia block (South China): new evidence for the Neoproterozoic breakup of Rodinia. Precambrian Res 187:263–276

Shu LS, Jahn BM, Charvet J, Santosh M, Wang B, Xu XS, Jiang SY (2014) Early Paleozoic depositional environment and intraplate tectono-magmatism in the Cathaysia block (South China): evidence from stratigraphic, structural, geochemical and geochronological investigations. Am J Sci 314:154–186

Shu L, Wang B, Cawood PA, Santosh M, Xu Z (2015) Early Paleozoic and early Mesozoic intraplate tectonic and magmatic events in the Cathaysia block, South China. Tectonics 34:1600–1621

Sun SS, McDonough WS (1989) Chemical and isotopic systematics of oceanic basalts: implications for mantle composition and processes. Geol Soc Lond, Spec Publ 42:313–345

Tam BM (2008) Vietnam magma Progress report from the tectonic point of view. Vietnam Institute of Geosciences and Mineral Resources, Ha Noi

Thanh TV, Hieu PT, Minh P, Nhuan DV, Thuy NTB (2019) Late Permian-Triassic granitic rocks of Vietnam: the Muong Lat example. Int Geol Rev 61:1823–1841

Thuc DD, Trung H (1995) Vietnam geology, part I of II: magma: Hanoi, Department of Geology and Mineral Resources Survey, 213–219 (In Vietnamese with English abstract)

Tran HT, Zaw K, Halpin JA, Manaka T, Meffre S, Lai CK, Lee Y, Van Le H, Dinh S (2014) The Tam Ky-Phuoc son shear zone in Central Vietnam: tectonic and metallogenic implications. Gondwana Res 26:144–164

Tri TV, Khuc V (2011) Geology and earth resources of Vietnam. Hanoi, Publishing House for Science and Technology, pp 634

Usuki T, Lan CY, Yui TF, Iizuka Y, Van Vu T, Tran TA, Okamoto K, Wooden JL, Liou JG (2009) Early Paleozoic medium-pressure metamorphism in Central Vietnam: evidence from SHRIMP U-Pb zircon ages. Geosci J13:245–256

Vuong NV, Tich VV, Bent H (2004) The application of the U-Pb TIMS method to the analyses of the crystallization age of Dai Loc massif. Vietnam J Earth Sci 26:202–207 (in Vietnam with English abstract)

Wang LJ, Griffin WL, Yu JH, O'Reilly SY (2013a) U–Pb and Lu–Hf isotopes in detrital zircon from Neoproterozoic sedimentary rocks in the northern Yangtze block: implications for Precambrian crustal evolution. Gondwana Res 23:1261–1272

Wang XL, Zhou JC, Griffin WL, Zhao G, Yu JH, Qiu JS, Zhang YJ, Xing GF (2014) Geochemical zonation across a Neoproterozoic orogenic belt: isotopic evidence from granitoids and metasedimentary rocks of the Jiangnan orogen, China. Precambrian Res 242:154–171

Wang X, Yuan C, Zhang Y, Long X, Sun M, Wang L, Soldner J, Lin Z (2018) S-type granite from the Gongpoquan arc in the Beishan

Orogenic collage, southern Altaids: implications for the tectonic transition. J Asian Earth Sci 153:206–222

Wang Y, Fan W, Zhao G, Ji S, Peng T (2007) Zircon U–Pb geochronology of gneissic rocks in the Yunkai massif and its implications on the Caledonian event in the South China block. Gondwana Res 12:404–416

Wang Y, Zhang A, Fan W, Zhang Y, Zhang Y (2013b) Origin of paleosubduction-modified mantle for Silurian gabbro in the Cathaysia block: Geochronological and geochemical evidence. Lithos 160:37–54

Wang Y, Zhang A, Fan W, Zhao G, Zhang G, Zhang Y, Zhang F, Li S (2011) Kwangsian crustal anatexis within the eastern South China block: geochemical, zircon U–Pb geochronological and Hf isotopic fingerprints from the gneissoid granites of Wugong and Wuyi–Yunkai domains. Lithos 127:239–260

Whitney DL, Evans BW (2010) Abbreviations for names of rock-forming minerals. Am Mineral 95:185–187

Wiedenbeck MAPC, Alle P, Corfu F, Griffin WL, Meier M, Oberli FV, Quadt AV, Roddick JC, Spiegel W (1995) Three natural zircon standards for U-Th-Pb, Lu-Hf, trace element and REE analyses. Geostand Geoanal Res 19:1–23

Wilson M (1989). Igneous Petrogenesis: a global tectonic approach. Springer, 466

Wu FY, Yang YH, Xie LW, Yang JH, Xu P (2006) Hf isotopic compositions of the standard zircons and baddeleyites used in U–Pb geochronology. Chem Geo 234:105–126

Wu Y, Zheng Y (2004) Genesis of zircon and its constraints on interpretation of U-Pb age. Chin Sci Bull 49:1554–1569

Xiang L, Shu L (2010) Pre-Devonian tectonic evolution of the eastern South China block: Geochronological evidence from detrital zircons. Sci China Earth Sci 53:1427–1444

Yu JH, O'Reilly SY, Wang L, Griffin WL, Zhang M, Wang R, Jiang S, Shu L (2008) Where was South China in the Rodinia supercontinent?: evidence from U–Pb geochronology and Hf isotopes of detrital zircons. Precambrian Res 164:1–15

Zhang A, Wang Y, Fan W, Zhang F, Zhang Y (2010) LA-ICPMS zircon U-Pb geochronology and Hf isotopic composition of Caledonian granites from the Qingliu area, Southwest Fujian. Geotecton Metallog 34:408–418

Zhang F, Wang Y, Zhang A, Fan W, Zhang Y, Zi J (2012) Geochronological and geochemical constraints on the petrogenesis of middle Paleozoic (Kwangsian) massive granites in the eastern South China block. Lithos 150:188–208

Zhou X, Yu JH, O'Reilly SY, Griffin WL, Wang X, Sun T (2017) Sources of the Nanwenhe-song Chay granitic complex (SW China-NE Vietnam) and its tectonic significance. Lithos 290:76–93

Zhu CL, Long B (1997) Evolution of granitoids in southern China. Geotecton Metallog 21:181–188 (in Chinese)